Numerical study of the effects of pressure on soot formation in laminar coflow n-heptane/air diffusion flames between 1 and 10 atm

Jean-Louis Consalvi, Fengshan Liu

Version of Record: https://www.sciencedirect.com/science/article/pii/S1540748920302595
Manuscript_59241c65f7fd66b089365b7d7c87d3b2

Effects of pressure on soot formation in laminar coflow methane/air diffusion flames doped with *n*-heptane and toluene between 2 and 8 atm

Mingyan Gu[1], Fengshan Liu[2], Jean-Louis Consalvi[3*], Ömer L. Gülder[4]

[1]School of Energy and Environment, Anhui University of Technology, Ma'anshan, China 243002

[2]Metrology Research Centre, National Research Council, 1200 Montreal Road, Ottawa, Ontario, Canada K1A 0R6

[3]Aix-Marseille Université, CNRS, IUSTI UMR 7343, 5 rue E. Fermi, 13013 Marseille, France.

[4]University of Toronto Institute for Aerospace Studies, 4925 Dufferin Street, Toronto, Ontario, Canada M3H 5T6

*Corresponding author: Jean-Louis Consalvi. Email: jean-louis.CONSALVI@univ-amu.fr

Abstract:

There is currently a lack of adequate understanding of soot formation in flames fueled with liquid hydrocarbons at elevated pressures. In this study, laminar coflow *n*-heptane and toluene doped CH_4/air diffusion flames were numerically investigated under a constant carbon mass flow rate at pressures between 2 and 8 atm to understand how pressure affects the sooting propensity of these two main components of surrogate fuels mimicking gasoline. Numerical simulations were performed using a detailed reaction mechanism containing 175 species and 1175 reactions and a sectional soot model. Soot inception is modeled by collisions among pyrene, BAPYR and BGHIF. Soot surface growth and oxidation are modeled using the hydrogen abstraction acetylene addition (HACA) mechanism as well as PAH surface condensation. The predicted sensitivity of soot production to pressure is in better agreement with the measurements of Daca and Gülder [2017] when the soot aging effect is considered in HACA surface growth. The predicted soot concentrations are in overall good agreement with measurements. Propargyl recombination and propargyl reaction with propyne are important pathways for the formation of benzene. In methane+toluene flames, attack of toluene by H radical is an effective benzene formation pathway low in the flame, but the relative importance

of benzene formation from toluene is reduced with increasing pressure. Although all the soot formation processes are enhanced with increasing pressure, PAH condensation is enhanced the most, followed by HACA and inception. At 6 and 8 atm, PAH condensation becomes comparable to HACA. The pressure dependence of the sooting propensity follows the order of methane+toluene < methane+*n*-heptane < methane, consistent with measurements. This result can be explained by the pressure dependence of benzene formation pathways, the kinetic effect of pressure, and the scrubbing effect of soot production on the gas-phase species involved in soot formation.

Key Words: Laminar coflow diffusion flame, gasoline surrogate components, soot production, elevated pressure, PAH-based soot model.

1. Introduction

Many combustion devices operate at elevated pressures for reasons of optimal efficiency and compact size. Soot formation is significantly enhanced at elevated pressures. Although significant progress has been made [1], our fundamental understanding of the pressure effects on the sooting propensity of different hydrocarbon fuels is still rather limited, particularly for liquid fuels.

Experimental studies have normally been conducted in buoyancy-controlled laminar coflow diffusion flames at elevated pressures by maintaining the same carbon mass flow rate in the fuel stream, so that both the flame heights and residence times remain nearly independent of pressure. Consequently, the soot quantities measured at the same heights above the burner at different pressures can be directly compared to reveal the pressure impact [1]. This methodology has been employed to investigate the effects of pressure on soot formation in laminar coflow diffusion flames of methane, ethane, ethylene, and propane as reviewed in [1]. A unified dependence of soot yield on pressure has been observed for methane, ethane and propane [2]. In the absence of a better depiction, the common practice has been to represent the scaling of the peak soot volume fraction with pressure

as $f_{v,\max} \propto P^n$, where the pressure exponent n seems to vary with both fuel and the range of pressure and displays poor agreement among available experimental studies [1]. For a given fuel, the pressure exponent n was found to decrease with increasing pressure [1].

Recent studies of soot formation in laminar coflow diffusion and partially-premixed flames at elevated pressures have focused on vaporized liquid fuels, in particular *n*-heptane [3-7], iso-octane [7], and toluene [6], due to their direct relevance to gasoline and diesel. Karataş et al. [3] conducted the first experimental study of soot temperature and volume fraction (f_v) in laminar coflow diffusion flames of nitrogen-diluted or helium-diluted vaporized *n*-heptane at pressures up to 7atm using the spectral soot emission (SSE) technique. They found that it is challenging to achieve very stable flames with increasing pressure. Based on their limited data of the maximum soot yield in nitrogen-diluted *n*-heptane diffusion flames, they concluded that soot formation in *n*-heptane flames are slightly more sensitive to pressure than that in aliphatic gaseous hydrocarbon flames at pressures up to 7atm. Daca and Gülder [6] conducted an experimental study to measure soot temperature and f_v distributions in laminar coflow CH_4/air diffusion flames with vaporized *n*-heptane doping up to 8atm and toluene doping up to 6 atm using SSE. Their results show that the toluene-doped methane flames display a higher sooting propensity than the *n*-heptane-doped methane flames over the pressure range investigated, consistent with the finding of Kashif et al. [8] in laminar coflow CH_4/air diffusion flames doped with *n*-heptane/toluene blends at atmospheric pressure. Moreover, their experimental results also suggest that the sooting propensity of toluene-doped methane flame displays a relatively weaker pressure dependence than that of *n*-heptane-doped methane flame. However, the mechanism for the weaker pressure dependence of the sooting propensity of toluene doped methane flame has not been investigated.

Due to experimental challenges that limit measurements at elevated pressures, numerical modeling plays an important role in understanding the pressure effects on soot formation. Previous numerical studies of soot formation in laminar coflow diffusion flames using detailed combustion chemistry

and polycyclic aromatic hydrocarbons (PAH) based soot models are limited to either gaseous hydrocarbon fuels at elevated pressures [9-13] or vaporized liquid hydrocarbon fuels at atmospheric pressure [14-19]. The only numerical studies to investigate soot formation in laminar coflow diffusion flames of a liquid fuel at elevated pressures are perhaps those of Consalvi and Liu [20] and Qiu et al. [21]. Consalvi and Liu simulated the nitrogen-diluted *n*-heptane diffusion flames at pressures from 1 to 10atm experimentally investigated by Karataş et al. [3] using detailed gas-phase chemistry and a sectional soot model. The predicted pressure dependence of the peak soot volume fraction agrees well with the data at pressures above 2atm and was found stronger than that for gaseous hydrocarbons over a similar pressure range. More recently, Qiu et al. [21] conducted a numerical study of soot formation in laminar coflow *n*-heptane-doped CH_4 diffusion flames at 4, 6, and 8 atm experimentally investigated by Daca and Gülder [6]. Their simulation was performed using the CoFlame code [22] along with a detailed kinetic model with PAH formation up to pyrene and a soot inception model based on dimerization of two pyrene molecules through collision. They found that the peak soot volume fraction scales with pressure as $P^{2.25}$ and $P^{1.60}$ for the pure CH_4 flame and for the *n*-heptane-doped CH_4 flame, respectively. They also showed that the primary particle number density, mean primary particle size, and the average primary particle number per aggregate all increase with increasing pressure. However, they did not investigate why the *n*-heptane-doped CH_4 flame displayed a weaker pressure dependence than the pure CH_4 flame. It has been widely accepted that the elevated pressure affects soot formation through enhanced density, narrowing of the flames, accelerated fuel pyrolysis due to enhanced air entrainment into the fuel stream near the burner rim [11,20,23], and hydrodynamics and mixing [13]. However, it has also been emphasized that pressure affects soot formation through modifying the gas-phase chemistry, in particular to reduce mole fractions of active radicals [12,20] and to alter the relative importance of benzene formation pathways [11].

In this study, the laminar coflow methane diffusion flames doped by *n*-heptane and toluene experimentally investigated in Ref. [6] were numerically simulated using detailed gas-phase chemistry with PAH formation up to five-rings and a sectional soot model. The objectives of this study are: (i) to investigate how pressure affects soot nucleation, surface growth, PAH condensation, and soot oxidation in laminar coflow *n*-heptane-doped and toluene-doped CH_4/air diffusion flames between 2 and 8 atm, (ii) to understand why the sooting propensity of the toluene-doped CH_4 flame has a weaker pressure dependence than that of the *n*-heptane-doped flame, and (iii) to demonstrate the importance of considering the soot aging effect in the HACA mechanism to the prediction of pressure dependence of soot formation at elevated pressures.

2. Numerical Model

2.1. CoFlame

Numerical simulations were conducted using the CoFlame code [22]. CoFlame solves the conservation equations of mass, momentum, energy, and gas-phase chemical species in axisymmetric cylindrical coordinates. Soot particle dynamics is modeled using a fixed sectional method. The transport equations of the number densities of aggregate and primary particle in all the sections are solved in a coupled fashion with the corresponding conservation equations. The soot chemistry and gas-phase chemistry are coupled through soot nucleation, surface growth by HACA and PAH condensation, and soot oxidation by O_2 and OH. Radiation heat transfer is taken into account. Details of the transport equations, the sectional soot model, and the radiation model can be found in [22].

2.2. Gas-phase mechanism

The shortened reaction mechanism for gasoline surrogate fuel employed previously is used [20]. It consists of 175 chemical species and 1086 reactions and includes PAHs up to 5-ring species.

2.3. Soot model

The fixed sectional soot model is described in detail in [22]. The range of soot aggregate mass is divided into a number of discrete sections of prescribed mass. In each section, all the soot aggregates are assumed to be identical and composed of equally sized spherical primary particles. All aggregates have a constant fractal dimension of 1.8. The evolution of each section is governed by two transport equations for the number densities of soot aggregate and primary particles. The incipient soot particles are assumed to be spherical and belong to the first section. Thirty-five sections were used with a spacing factor of 2.35.

Dimers of PAHs formed by collisions are likely unstable at flame temperatures around 1600 K [24,25]. Instead, dimers of PAHs at flame temperatures are formed primarily through reactive dimerization [26]. However, due to the absence of well-established soot nucleation models based on reactive PAH dimerization, soot nucleation was modeled through the collision and sticking of two PAH molecules to form a dimer and the reversibility of the soot nucleation process [27] was not considered in this study. The nucleation rate is calculated as [22]:

$$\left.\frac{\partial N_1^a}{\partial t}\right|_{nu} = \left.\frac{\partial N_1^p}{\partial t}\right|_{nu} = \beta\sqrt{\frac{8\pi k_B T}{\mu_{AB}}}(r_A + r_B)^2 A_v^2[A][B] \tag{1}$$

N_1^a, N_1^p, β, k_B,, μ_{AB} and r_A and r_B are the aggregate and primary particle number densities, the nucleation efficiency, the Boltzmann constant, the collisional reduced mass for the two colliding PAHs A and B and their radii, respectively. A_v is Avogadro's number, and [A] and [B] are the PAH molar concentrations. In CoFlame, soot nucleation was modeled as a result of collisions among three five-ring PAHs, namely benzo[a]pyrene (BAPYR), secondary benzo[a]pyrenyl (BAPYR*S), and benzo(ghi)fluoranthene (BGHIF) and β was set to 0.0001 [22]. In this study, soot nucleation was assumed to result from collisions among pyrene (A_4), BAPYR and BGHIF and the parameter β was set to 0.002. These modifications were found necessary to reproduce reasonably well the measured peak soot volume fractions of Ref. [6] over the pressure range considered when the shortened toluene

reference fuel reaction mechanism [20] was used and can be rationalized by our limited understanding of soot nucleation and large uncertainty in PAH formation chemistry.

In this study, the PAH condensation growth of soot particles was contributed by all the three soot nucleation PAH species (A4, BAPYR, and BGHIF) and the condensation efficiency was assigned to be unity. An important parameter in modeling the HACA surface growth is the steric factor α, which represents the fraction of reactive sites on soot surface and is also used to model the soot aging phenomenon. Different values and expressions of α have been used, e.g. [28], due mainly to large uncertainties in modeling soot nucleation rate and PAH chemistry. In this study, two sets of numerical simulation were carried out: one used a constant value of α=0.3 (without considering soot aging, Model 1), the other used a primary particle diameter, d_p, dependent expression $\alpha=\exp[-1.2(d_p/d_{p,0})^2]$. $d_{p,0}$ is a reference primary particle diameter and was set to 8nm in this study (Model 2). In Model 2, α is higher than 0.95 for newly formed soot particles less than 2nm but decreases rapidly with increasing d_p to become negligible above 15nm.

2.4. Computational details

This study intends to simulate the flames investigated experimentally in Ref. [6]. The burner consists of two concentric steel tubes of 3mm and 25.4mm inner diameter. The laminar coflow diffusion flames were fueled with pure methane, *n*-heptane-doped methane, and toluene-doped methane. The total carbon mass flow rate was kept constant at 0.41mg/s. A small amount of vaporized *n*-heptane and toluene was added separately to the methane stream, resulting in 7.5% of the total carbon mass from *n*-heptane or toluene. The fuel stream and the coflow air were heated to 230°C and 200°C, respectively. The pressure range of the experiments was 1 to 6 atm for the toluene-doped methane flames and 1 to 8 atm for the *n*-heptane-doped flames, limited by flame stability.

Numerical simulation was performed at 2, 4, 6 and 8atm for all the flames considered. Calculations were conducted in a domain of 1.66cm (z)×1.14cm (r) with 130 (z)×85 (r) non-uniform control

volumes. The computational meshes are fine in the near burner exit region and then become gradually coarser with increasing radial and streamwise coordinates. When methane is doped with *n*-heptane or toluene, the dopant mole fraction in the fuel stream is 0.0128. At the fuel stream inlet, a parabolic velocity profile was assumed with a mean stream velocity of 20.163/*P* for the neat methane flames and 18.70/*P* cm/s (*P* in atm) for doped methane flames. At the air stream, a uniform velocity of 91.55/*P* cm/s was imposed.

3. Results and Discussion

3.1. Flame shape

The predicted flame shapes of the doped methane flames between 2 and 8atm display the well-known behavior and are in overall good agreement with the experimental observations in [6]: with increasing *P* the flames become narrower and the flame heights remain nearly constant with a slight increase. A quantitative comparison of the flame heights is shown in Fig. 1. The numerical flame height is defined as the axis location where the temperature peaks, while the experimental flame height is based on the luminosity of soot emissions inferred from the flame photos [11]. The predicted flame heights in the doped methane flames increase slightly with pressure at nearly the same rate. However, the experimental flame heights display a weaker sensitivity to pressure. This discrepancy is likely due to the neglect of the fuel preheat effect [19] as well as the tapered fuel tube exit [6] in the modeling. A slightly higher flame height of the toluene-doped flames is well reproduced numerically. The small increase in flame height with increasing pressure suggests that soot quantities at a given height in the soot formation region can be directly compared in these buoyancy-controlled flames.

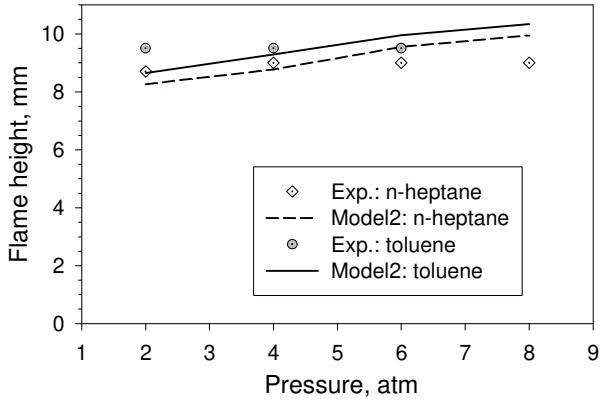

Fig. 1. Flame heights as a function of pressure for the *n*-heptane- and toluene-doped methane diffusion flames.

3.2. Pressure effects on temperature and soot production

Soot quantities in laminar flames are determined by residence time, flame temperature, and chemical environment. In the context of this study, the temperature distributions in the *n*-heptane- and toluene-doped methane diffusion flames were found to be very similar, since *n*-heptane and toluene contribute only 7.5% to the total carbon mass.

The effect of pressure on soot production can be assessed using different quantities, such as $f_{v,max}$ [6], the maximum soot yield [6], and the total soot loading [4,5,7]. The predicted and measured values of $f_{v,max}$ are compared in Fig. 2. Both the measured and predicted results of $f_{v,max}$ indicate that soot formation is enhanced with increasing pressure and with the doping of *n*-heptane and toluene and follow the order of $\text{methane} < \text{methane} + \text{n} - \text{heptane} < methane + \text{toluene}$. While this order can be explained in terms of the concentrations of PAHs, it is also consistent with the H/C ratio of the fuel mixture. In addition, both Models 1 and 2 capture the overall pressure dependence and the relative sooting propensity of methane and *n*-heptane- and toluene-doped methane flames. Moreover, Model 2, which considers the aging effect of HACA surface growth, predicts higher and lower $f_{v,max}$ at low and high pressures, respectively, than Model 1. While Model 1 predicts a stronger pressure dependence of the $f_{v,max}$ than the experimental data, Model 2 predicts the pressure dependence of

$f_{v,max}$ in better agreement with the data. The sooting propensity of toluene-doped methane flame remains the highest over the pressure range considered. An interesting feature of Fig. 2 is that the overall pressure dependence of the $f_{v,max}$ follows the order of $\text{methane} > m\text{ethane} + \text{n} - \text{heptane} > \text{methane} + \text{toluene}$ from both experimental data and numerical results. It is noticed that the order of overall pressure dependence of $f_{v,max}$ of the three flames remains the same in the results of both Model 1 and Model 2. Moreover, this conclusion is found independent of the particular choice of collision efficiency β and the reference primary particle diameter $d_{p,0}$ in Model 2 as shown in Supplemental Material S1. Although this feature was noticed in Ref. [6], the mechanisms responsible for this phenomenon remains unexplained.

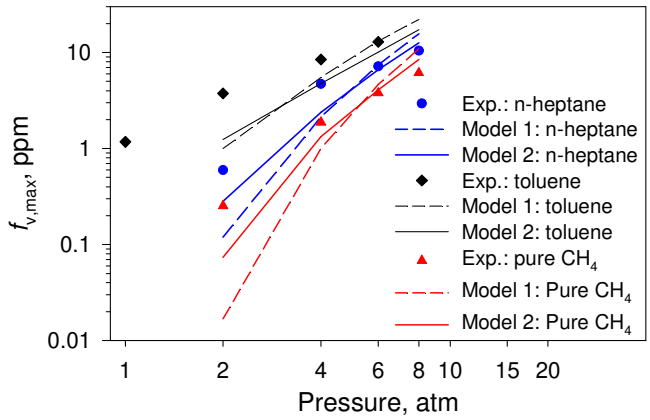

Fig. 2. Predicted and measured maximum $f_{v,max}$ in methane, $\text{methane} + n - \text{heptane}$, and $\text{methane} + \text{toluene}$ flames.

The pressure dependence of the $f_{v,max}$ in laminar flames has often been described as $f_{v,max} \propto P^n$. The predicted by Model 2 and measured values of the pressure exponent n are compared in Table 1. It is clear from Fig. 2 and Table 1 that the pressure dependence of $f_{v,max}$ of the methane flame becomes increasingly weaker with doping by *n*-heptane and toluene over the entire pressure range investigated

(the last two rows of Table 1). Although Model 2 over-predicts the pressure exponents, it captures the increasingly reduced pressure dependence with *n*-heptane and toluene doping.

Table 1. Pressure exponents based on $f_{v,max}$.

P(atm) range	Source	CH_4	CH_4 + *n*-heptane	CH_4 + toluene
2 to 4	Model 2	4.17	3.08	1.94
	Exp.	2.88	2.98	1.68[a]
4 to 8	Model 2	2.67	2.41	1.88
	Exp.	1.71	1.14	1.13[b]
2 to 8	Model 2	3.44	2.78	1.90
	Exp.	2.31	2.07	1.33[c]

[a]1 to 2 atm. [b]2 to 6 atm. [c]1 to 6 atm.

Although $f_{v,max}$ has often been used to quantify the pressure dependence of sooting propensity of fuels, this practice does not consider the fact that the location of $f_{v,max}$ shifts from the flame centerline at lower pressures to the flame wing at sufficiently high pressures. Following Gülder and co-workers, the soot yield can be used to better quantify the pressure dependence of soot production. The soot yield is calculated as [6]:

$$Y_s(z) = \rho_s \int 2\pi r f_v(r,r)\, v(r,r) dr / \dot{m}_c \qquad (2)$$

where ρ_s=1.8 g/cm^3 is the soot density, v_z is the axial velocity and $\dot{m}_c$ is the carbon mass flow rate at the nozzle exit (0.41 mg/s). The numerator of Eq. (2) denotes the soot mass flow at a given axial height *z*. To minimize the discrepancy between predicted and measured soot yield, the axial velocity was calculated in the same way as in [6], i.e., $v(r,z)=(2az)^{0.5}$ with a=41 m/s^2. The calculated maximum soot yields by Model 2 shown in Fig. 3 compare favorably with the experimental data [6]. Overall, Fig. 3 displays similar features to Fig. 2 with regard to the performance of Model 2 and the

relative pressure dependence of the three flames. The pressure exponents based on the maximum soot yield are lower than those based on $f_{v,max}$, consistent with previous studies summarized in [1].

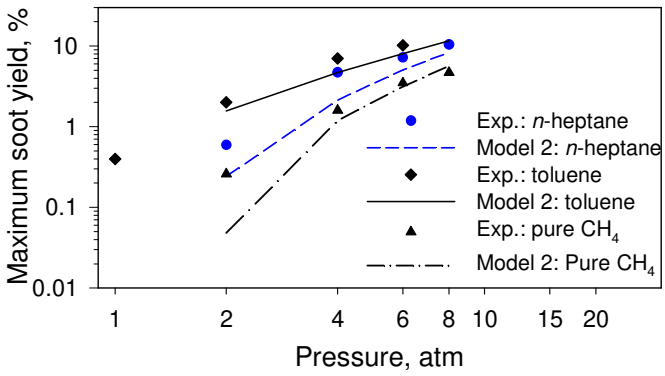

Fig. 3. Predicted and measured maximum soot yields in all the three flames.

To further evaluate the pressure dependence of the sooting propensity of the doped and undoped methane flames, the total soot loading (integration of f_v over the entire flame) in each of the flame between 2 and 8 atm was calculated. The pressure exponents based on the maximum soot yield, soot loading, and the maximum f_v in the three flames between 4 and 8 atm are summarized in Table 2. Although the pressure exponents vary somewhat with the soot quantity considered, the relative pressure dependence remains consistently the same, i.e., $\text{methane} > \text{methane} + \text{n} - \text{heptane} > \text{methane} + \text{toluene}$.

Table 2. Pressure exponents of the maximum soot yield, soot loading, and $f_{v,\,max}$ by Model 2 over 4 to 8 atm.

Flames	Max. soot yield	Soot loading	Max. f_v
CH_4	2.26	2.56	2.67
CH_4+*n*-heptane	1.97	2.30	2.41
CH_4+toluene	1.32	1.52	1.88

To illustrate the overall level of quantitative agreement between predicted (Model 2) and measured f_v, Fig. 4 compares the radial distributions of predicted and measured f_v in the *n*-heptane-doped methane flames at three representative heights: low in the flame where soot particles form in an annular region through nucleation and surface growth (z=3 mm), near the middle of the flame where f_v is close to the maximum (z=6 mm), and higher in the flame where soot oxidation dominates (z=8 mm). The two-dimensional distributions of f_v predicted by Model 2 in all the flames studied at the four pressures are provided in Supplemental Material S2.

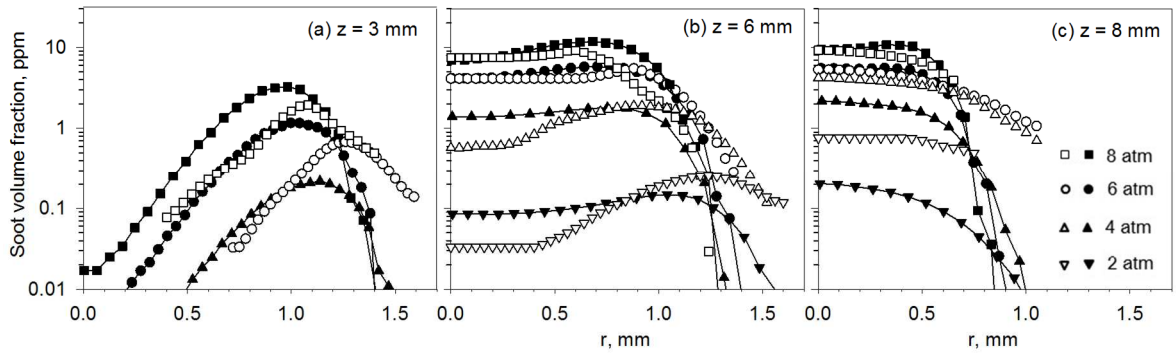

Fig. 4. Calculated (solid symbols: Model 2) and measured (open symbols) radial distributions of f_v at z=3, 6, and 8 mm in the *n*-heptane-doped methane flame between 2 and 8 atm.

Experimental data of soot volume fraction are unavailable at z=3 mm. At z=3 mm the predicted f_v peaks at a slightly smaller radial position compared to measurements, Fig. 4(a). This discrepancy might be attributed to the neglect of the tapered burner tip in the modeling. Nevertheless, the model captures the main features of the experiments in terms of level and distributions. For example, at z=6 and 8 mm the values of f_v at the flame centerline regions at P=6 and 8 atm are quantitatively well predicted, Figs. 4(b) and 4(c). The predicted f_v distributions are in overall much improved agreement with measurements compared to our previous study [20], especially in the flame centerline region, which is largely attributed to the improved soot nucleation and PAH condensation sub-models. With increasing pressure, the f_v peak moves toward the flame centerline and f_v increases due to both flame

narrowing, enhanced fuel pyrolysis, and enhanced PAH production hydrodynamically and kinetically.

3.3. Pressure effects on soot production rates

To explore the causes of the decreased pressure dependence of soot formation in *n*-heptane-doped and toluene-doped methane flames, Fig. 5 shows the normalized maximum rates of soot nucleation, HACA surface growth, and PAH condensation between 2 and 8 atm. The rates are normalized by the respective values at 2 atm. The two-dimensional distributions of the rates of the three soot production processes in all the flames investigated are shown in Supplemental Material S3. The small decrease in the normalized maximum nucleation rate of the toluene-doped methane flame at P=4 atm does not mean that pressure reduces the overall soot nucleation. Rather, in this case, soot nucleation displays double peaks near the flame centerline region (Supplemental Material S3) and is a result of the distributions of the three PAHs shown in Supplemental Material S5. It is evident that all the three processes contributing to soot production are enhanced with increasing pressure and their sensitivity to pressure follows the order: $\text{PAH condensation} > \text{HACA surface growth} > \text{nucleation}$. Among the flames of methane, methane+*n*-heptane, and methane+toluene, the enhancement in all the three soot formation processes by pressure follows the same order as the pressure dependence of $f_{v,max}$ shown in Fig. 2 and Table 1, namely $\text{methane} > \text{n} - \text{heptane} - \text{doped methane} > \text{toluene} - \text{doped methane}$. Therefore, the decreased pressure dependence of $f_{v,max}$ shown Fig. 2 with the doping of *n*-heptane and toluene is a direct result of the reduced enhancement in all the soot production processes with increasing pressure.

Soot mass production is predominately attributed to soot surface growth by HACA and PAH condensation (Supplementary Material S3). Although HACA plays a significantly more important role than PAH condensation at 2 and 4 atm, PAH condensation plays a similar role to soot surface growth to HACA at 6 and 8 atm, regardless if the methane flame is doped or not (Supplementary

Material S3). Moreover, PAH condensation dominates surface growth in the flame centerline region while HACA is dominant along the flame wing (Supplemental Material S3). The enhanced role of PAH condensation with increasing pressure is attributed to the higher production of PAH and larger soot particle sizes. Increasing pressure affects the flame kinetically by prompting three-body recombination reactions and suppressing the most important radicals, i.e., O, OH, and H, especially H radicals, see [12] and Supplemental Material S4. Increasing pressure favors the production of larger hydrocarbons and PAHs [11]. The weaker suppression of OH than H by pressure implies that the relative importance of OH to PAH and soot oxidation is enhanced. The significant consumption of H radicals with pressure explains the reduced relative importance of HACA to soot surface growth. The enhancement of both PAH condensation and HACA by pressure gradually levels off with increasing pressure, especially PAH condensation. The level-off of PAH condensation and HACA surface growth rates with increasing pressure is caused by the scrubbing effect of soot formation on the gas-phase species concentrations.

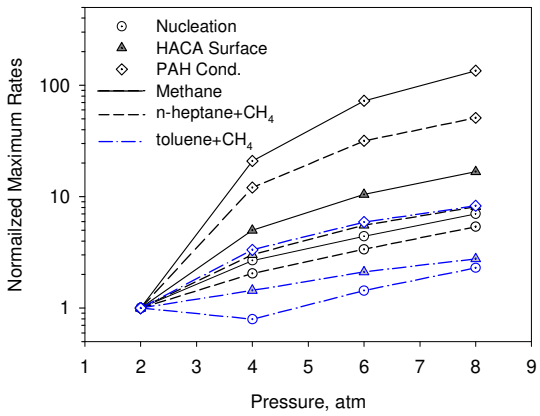

Fig. 5. Variation of the normalized maximum rates of soot nucleation, HACA surface growth, and PAH condensation with pressure.

3.4 Pressure effects on the molar concentrations of species involved in soot formation

To understand the different pressure dependence of the soot production processes in the undoped and doped methane flames, the pressure dependence of molar concentrations of species involved in soot

formation is examined. The normalized maximum molar concentrations of H, C_2H_2, A_4, BAPYR, BGHIF, C_3H_3, and A_1 by the corresponding values at 2 atm are plotted in Fig. 6. If there were no chemical effects due to pressure and scrubbing of gaseous species by soot formation, the species molar concentrations should increase linearly with *P* as indicated by the dotted lines. The results shown in Fig. 6 indicates that the chemical effects associated with increasing the pressure and scrubbing of C_2H_2 and PAHs strongly suppress almost all these species, except A_1 in all the three flames and BGHIF in the pure methane flame below 8 atm. In particular, H is strongly suppressed by pressure in all three flames due to the enhanced three-body recombination reactions. The two five-ring PAHs, BGHIF and BAPYR, are also significantly suppressed with increasing pressure, except BGHIF in the pure methane flame. To understand the variation of the normalized molar concentrations of A_4, BGHIF and BAPYR with pressure, the computed 2D distributions of molar concentration of these three PAHs at *P*=2, 4, 6, and 8 atm using Model 2 are shown in Supplemental Material S5 along with a brief discussion of those results based on a reaction pathway analysis.

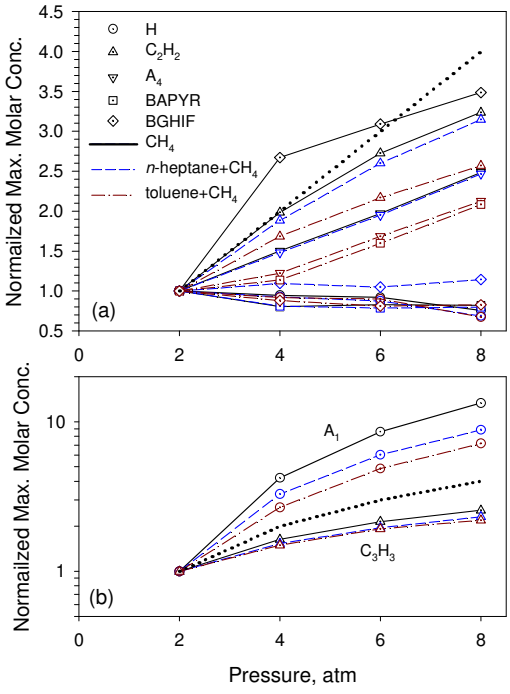

Fig. 6. Pressure dependence of the normalized maximum molar concentrations of H, C_2H_2, A_4, BAPYR, and BGHIF, (a), and C_3H_3 and A_1, (b).

The formation of benzene (A_1) is critical to the subsequent formation of PAHs and soot. Although the normalized maximum molar concentrations of A_1 in all the three flames also display reduced pressure dependence as the pressure increases, i.e., the slope of normalized $[A_1]_{max}$ decreases with increasing P, A_1 is actually prompted kinetically by pressure, Fig. 6(b). This is because increasing pressure favors the formation of larger hydrocarbons, A_1, and PAHs and A_1 does not directly participate in soot nucleation or surface growth. A pathway analysis shows that A_1 is primarily formed through recombination of propargyl (R332: $C_3H_3 + C_3H_3 \leftrightarrow A_1$) and propargyl reaction with propyne (R336: $C_3H_3 + C_3H_4 \leftrightarrow A_1 + H$) in the pure methane and methane+*n*-heptane flames. Although doping of methane by *n*-heptane increases A_1 formation, the linear structure of *n*-heptane molecules [16] does not form A_1 effectively. On the other hand, in methane+toluene flames, the direct attack of H radicals on the ring-structured toluene molecules [16] low in the flame wing through R372 ($C_7H_8 + H \leftrightarrow A_1 + CH_3$) provides a very efficient pathway to A_1 formation. In fact, R372 is the most important reaction to A_1 formation in the methane+toluene flame at 2 atm. However, with increasing pressure the rates of R332 and R336 increase rapidly but the rate of R372 decreases modestly and at P=8 atm the rate of R332 exceeds the rate of R372. Therefore, the relative importance of toluene attack by H to A_1 formation is reduced by increasing pressure. This is another important factor for the relative weaker pressure dependence of soot production in the methane+toluene flame.

4 Conclusions

Laminar axisymmetric coflow methane, methane+*n*-heptane, and methane+toluene diffusion flames at constant carbon mass flow rate between 2 and 8 atm were simulated to gain insights into the

effects of *n*-heptane and toluene doping to methane on the pressure dependence of PAH and soot formation. Numerical results are in fairly good agreement with experimental data. The following conclusions can be drawn:

1) The model reproduces the experimentally observed sooting propensity and the relative pressure dependence of methane, methane+*n*-heptane, and methane+toluene flames, especially when the soot aging effect was considered through a soot particle size dependent steric factor.
2) All three soot production processes (nucleation, HACA, and PAH condensation) are enhanced by increasing pressure; however, PAH condensation displays the largest sensitivity to pressure followed by HACA and then nucleation. PAH condensation dominates in the flame centerline region while HACA contributes the most along the flame wing.
3) The chemical enhancement of soot formation by pressure can be attributed to the enhanced three-body recombination reactions, suppressed formation of radicals, and increased formation of PAHs. The reduced pressure dependence of soot loading with increasing pressure is due to the scrubbing effect of soot formation on gas-phase species.
4) Propargyl recombination and propargyl reaction with propyne are important pathways of benzene formation. The attack of toluene by H also plays an important role in benzene formation low in the flame of methane+toluene. However, the former pathways are strongly enhanced while the latter is modestly weakened with increasing pressure.
5) The reduced pressure dependence of soot loading in the methane flame by *n*-heptane and toluene doping can be explained by the pressure dependence of the rates of the three soot production processes, which in turn are determined by the pressure dependence of H and benzene formation and the scrubbing effect of soot formation and gas-phase species involved in soot formation.

Acknowledgements

MG would like to thank the support of Natural Science Foundation of China (project number: 51776001).

References

[1] A.E. Karataş, Ö.L. Gülder, Soot formation in high pressure laminar diffusion flames, Prog. Ener. Combust. Sci. 38 (2012) 818-845.

[2] Ö.L. Gülder, G. Intasopa, H.I. Joo, P.M. Mandatori, D.S. Bento, M.E. Vaillancourt, Unified behaviour of maximum soot yields of methane, ethane and propane laminar diffusion flames at high pressures, Combust. Flame 158 (2011) 2037–2044.

[3] A.E. Karataş, G. Intasopa, Ö.L. Gülder, Sooting behaviour of n-heptane laminar diffusion flames at high pressures, Combust. Flame 160 (2013) 1650-1656.

[4] L. Zhou, N.J. Dam, M.D. Boot, L.P.H. de Goey, Measurements of sooting tendency in laminar diffusion flames of n-heptane at elevated pressure, Combust. Flame 160 (2013) 2507-2516.

[5] L. Zhou, G. Xiong, M. Zhang, L. Chen, S. Ding, L.P.H. de Goey, Experimental study of polycyclic aromatic hydrocarbons (PAHs) in n-heptane laminar diffusion flames from 1 to 3 bar, Fuel 209 (2017) 265-273.

[6] A.E. Daca, Ö.L. Gülder, Soot formation characteristics of diffusion flames of methane doped with toluene and *n*-heptane at elevated pressures, Proc. Combust. Inst. 36 (2017) 737-744.

[7] S. Liang, Z. Li, J. Gao, X. Ma, H. Xu, S. Shuai, PAHS and soot formation in laminar partially premixed co-flow flames fueled by PRFs at elevated pressures, Combust. Flame 206 (2019) 363-378.

[8] M. Kashif, J. Bonnety, A. Matynia, P. Da Costa, G. Legros, Sooting propensities of some gasoline surrogate fuels: combined effects of fuel blending and air vitiation, Combust. Flame 162 (2015) 1840-1847.

[9] N.A. Eaves, A. Veshkini, C. Riese, Q. Zhang, S.B. Dworkin, M.J. Thomson, A numerical study of high pressure, laminar, sooting, ethane-air coflow diffusion flames, Combust. Flame 159 (2012) 3179-3190.

[10] N.A. Eaves, M.J. Thomson, S.B. Dworkin, The effect of conjugate heat transfer on soot formation modeling at elevated pressures, Combust. Sci. Technol. 185(12) (2013) 1789-1819.

[11] H. Guo, Z. Gu, K.A. Thomson, G.J. Smallwood, F.F. Baksh, Soot formation in a laminar ethylene/air diffusion flame at pressures from 1 to 8 atm, Proc. Combust. Inst. 34 (2013) 1795-1802.

[12] F. Liu, A.E. Karataş, Ö.L. Gülder, M. Gu, Numerical and experimental study of the influence of CO_2 and N_2 dilution on soot formation in laminar coflow C_2H_4/air diffusion flames at pressures between 5 and 20 atm, Combust. Flame 162 (2015) 2231-2247.

[13] A. Abdelgadir, I.A. Rakha, S.A. Steinmetz, A. Attili, F. Bisetti, W.L. Roberts, Effects of hydrodynamics and mixing on soot formation and growth in laminar coflow diffusion flames at elevated pressures, Combust. Flame 181 (2017) 39-53.

[14] M. Saffaripour, P. Zabeti, S.B. Dworkin, Q. Zhang, H. Guo, etc., A numerical and experimental study of a laminar sooting coflow Jet-A1 diffusion flame, Proc. Combust. Inst. 33 (2011) 601-608.

[15] A. Khosousi, F. Liu, S.B. Dworkin, N.A. Eaves, M.J. Thomson, etc., Experimental and numerical study of soot formation in laminar coflow diffusion flames of gasoline/ethanol blends, Combust. Flame 162 (2015) 3925-3933.

[16] J.-L. Consalvi, F. Liu, M. Kashif, G. Legros, Numerical study of soot formation in laminar coflow methane/air diffusion flames doped by *n*-heptane/toluene and isooctane-toluene blends, Combust. Flame 180 (2017) 167-174.

[17] T. Zhang, L. Zhao, M.R. Kholghy, S. Thion, M.J. Thomson, Detailed investigation of soot formation from jet fuel in a diffusion flame with comprehensive and hybrid chemical mechanisms, Proc. Combust. Inst. 37 (2019) 2037-2045.

[18] C. Chu, T. Zhang, M.J. Thomson, The chemical structure effects of alkylbenzenes on soot formation in a co-flow flame, Combust. Flame 204 (2019) 237-249.

[19] C. Zhang, L. Chen, S. Ding, H. Xu, G. Li, J.-L. Consalvi, F. Liu, Effects of soot inception and condensation PAH species and fuel preheating on soot formation modeling in laminar coflow CH4/air diffusion flames doped with n-heptane/toluene mixtures, Fuel 253 (2019) 1371-1377.

[20] J.-L. Consalvi, F. Liu, Numerical study of the effects of pressure on soot formation in laminar coflow *n*-heptane/air diffusion flames between 1 and 10 atm, Proc. Combust. Inst. 35 (2015) 1727-1734.

[21] L. Qiu, Y. Hua, X. Cheng, Y. Zhuang, Y. Qian, Numerical investigation of soot formation in a methane diffusion flame doped with *n*-heptane at elevated pressure, Energy Fuels 33 (2019) 11941-11947.

[22] N.A. Eaves, Q. Zhang, F. Liu, H. Guo, S.B. Dworkin, M.J. Thomson, CoFlame: a refined and validated numerical algorithm for modeling sooting laminar coflow diffusion flames, Comput. Phys. Commun. 207 (2016) 464-477.

[23] F. Liu, K.A. Thomson, H. Guo, G.J. Smallwood, Numerical and experimental study of an axisymmetric coflow laminar methane-air diffusion flame at pressures between 5 and 40 atmospheres, Combust. Flame 164 (2006) 456–471.

[24] H. Sabbah, L. Biennier, S.J. Klippenstein, I.R. Sims, B.R. Rowe, Exploring the role of PAHs in the formation of soot: pyrene dimerization, J. Phys. Chem. Lett. 1(19) (2010) 2962-2967.

[25] Q. Mao, A.C.T. van Duin, K.H. Luo, Formation of incipient soot particles from polycyclic aromatic hydrocarbons: A reaxFF molecular dynamics study, Carbon 121 (2017) 380-388.

[26] M.R. Kholghy, G.A. Kelesidis, S.E. Pratsinis, Reactive polycyclic aromatic hydrocarbon dimerization drives soot nucleation, Physical Chemistry Chemical Physics 20(16) (2018) 10926-10938.

[27] M.R. Kholghy, N.A. Eaves, A. Veshkini, M.J. Thomson, The role of reactive PAH dimerization in reducing soot nucleation reversibility, Proc. Combust. Inst. 37(1) (2019) 1003-1011.

[28] A. Veshkini, S.B. Dworkin, M.J. Thomson, A soot particle surface reactivity model applied to a wide range of laminar ethylene/air flames, Combust. Flame 161 (2014) 3191-3200.